integral value obtained with this method results very close to that obtained with the potential/boundary-layer simulation. However, it seems that the better prediction of the local behavior of the friction drag is obtained with the Reynolds-stress closure method. Note that for the RANS simulations the values of c_f obtained on both the upper and lower airfoil surfaces are reported. Because symmetry is not perfect, because of discretization errors, two slightly different lines can be distinguished.

In Fig. 1b, the local friction drag coefficient distributions obtained by the RANS and the boundary-layer methods are compared to the theoretical results for the flat plate. In both cases, the friction drag on the profile is higher than that on the flat plate in the leading-edge zone, although it is lower near the trailing edge. This behavior is consistent with the effects of the chordwise pressure gradient. Because the pressure distributions are practically the same in all of the simulations, the Reynolds-stress closure method predicts a larger variation of the local coefficient c_f with the pressure gradient than the potential/boundary-layer simulation. However, it is expected that RANS simulations give a better representation of the effects of the pressure gradient than the boundary-layer method; thus, it is not clear which solution is the most accurate in the leading-edge region.

The computations were carried out on a Pentium III 500-MHz XION processor, with 512 MB RAM. The computing time for the case with 34,000 total cells was about 70 min for the standard k–ε closure method, 110 min for the RNG k–ε closure method, and 150 min for the Reynolds-stress closure method (with a few seconds for the potential/boundary-layer simulations). Therefore, the Reynolds-stress closure method appears significantly more time consuming. In general, the RANS calculations seem to require computational resources, both memory and computing time, which would become prohibitive in three-dimensional calculations.

Conclusions

The capabilities of a solver of the RANS equations in predicting the friction drag over an airfoil have been investigated through comparison with the values given by a coupled potential/boundary-layer method, for different Reynolds numbers.

Preliminarily, the near-wall grid resolution required to obtain the grid independence of the friction drag in the RANS calculations has been assessed. It appears that, for all of the considered Reynolds numbers, a large amount of computational points is required, which would lead to an unaffordable mesh size in three-dimensional simulations.

Even on these highly refined grids, the value of the global C_F is overestimated by all of the turbulence models because they are not able to predict the boundary-layer transition. If comparison is made with the value given by the potential code coupled with a fully turbulent boundary layer, satisfactory agreement is obtained with the RNG k–ε and the Reynolds-stress closure models. The best global agreement is given by the RNG k–ε model. However, from the analysis of the chord distribution of the local c_f, it appears that this is due to compensation between an overestimate near the leading edge and an underestimation at the trailing edge.

The best local agreement is obtained, as expected, with the Reynolds-stress model; the only significant discrepancy with the BLOWS results is a less steep decrease of the c_f near the leading edge. Because the pressure distribution is almost identical, it appears that the RANS simulation with this closure models predicts larger variations of the friction coefficient with the pressure gradient. Because the boundary-layer solvers are not well suited for flows with high-pressure gradients, it is not clear whether the value of c_f obtained by potential/boundary-layer simulation is indeed more accurate in the region near the leading edge.

Finally, the RANS simulations require in general large computational time, and this increases significantly with the accuracy of the turbulence closure model. Thus, this analysis indicates that an accurate prediction of the friction drag around complex aeronautical configurations by RANS methods remains an extremely difficult task with the present computer capabilities.

References

[1] Lombardi, G., Morelli, M., and Salvetti, M. V., "Appraisal of Numerical Methods in Predicting the Aerodynamics of Forward Sweep Wings," *Journal of Aircraft*, Vol. 35, No. 4, 1998, pp. 561–568.

[2] Lombardi, G., Salvetti, M. V., Talamelli, A., "Shock-Wave/Boundary-Layer Interaction in Transonic Flow Around a Forward-Swept Wing," AIAA Paper 97-1838, June 1997.

[3] Launder, B. E., and Spalding, D. B., *Lectures in Mathematical Models of Turbulence*, Academic, London, 1972.

[4] Yakhot, V., and Orszag, S. A., "Renormalization Group Analysis of Turbulence: I. Basic Theory," *Journal of Scientific Computing*, Vol. 1, No. 1, 1986, pp. 1–51.

[5] Launder, B. E., "Second-Moment Closure: Present . . . and Future?," *International Journal of Heat Fluid Flow*, Vol. 10, No. 4, 1989, pp. 282–300.

[6] Baricci, A., "Procedura di Calcolo dell'Interazione Strato Limite-Flusso Potenziale su Profili Alari," Tesi di Laurea in Ingegneria Aeronautica, Univ. of Pisa, Italy, Nov. 1989.

[7] Abbott, I. H., and Von Doenhoff, A., *Theory of Wing Section*, Dover, New York, 1949.

Boundary-Layer Transition, Separation, and Reattachment on an Oscillating Airfoil

T. Lee* and G. Petrakis†
McGill University, Montreal, Quebec H3A 2K6, Canada
and
F. Mokhtarian‡ and F. Kafyeke§
Bombardier Aerospace,
Montreal, Quebec H3C 3G9, Canada

Introduction

CONSIDERABLE effort[1–10] has been made to investigate the flow structure around an airfoil with unsteady motions to advance the understanding of the unsteady flows developed on aerodynamic objects in unsteady motion and to continue the development and validation of predictive methods. An excellent review on unsteady aerodynamics is given by McCroskey.[11] Recently, the spatial–temporal progression of the boundary-layer events (i.e., the locations of leading-edge stagnation, transition, separation, and reattachment points) that occurred on a sinusoidally oscillated NACA 0012 airfoil model was identified nonintrusively by Lee and Basu[12] using multiple hot-film sensor arrays. However, due to the limitations of their experimental setup, only low-frequency/small-amplitude oscillations were investigated. In the present experiment, the effects of large oscillation frequency $0.05 \leq \kappa (= \pi f_0 C / U_\infty$, where f_0 is the oscillation frequency, C is the chord length, and U_∞ is the freestream velocity) ≤ 0.30 and amplitude (both within, through, and well beyond the static-stall angle of attack α_{ss}) on the unsteady boundary layer developed on an NACA 0012 airfoil model oscillated sinusoidally were examined using multiple hot-film sensor arrays. The hot-film measurements were then used to postulate the mechanisms responsible for these boundary-layer events.

Experimental Methods and Apparatus

The experiments were performed in a 60 cm × 90 cm × 1.8 m low-speed wind tunnel. An NACA 0012 airfoil, fabricated from

Received 14 May 1999; revision received 3 August 1999; accepted for publication 30 August 1999.

*Assistant Professor, Department of Mechanical Engineering.
†Graduate Student, Department of Mechanical Engineering.
‡Section Chief, Advanced Aerodynamics.
§Manager, Advanced Aerodynamics.

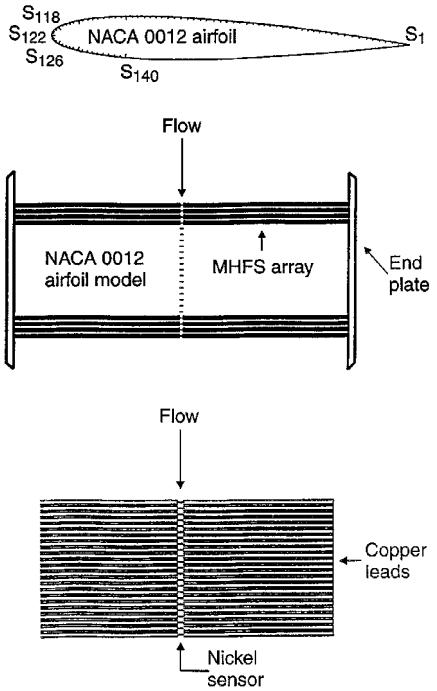

Fig. 1 Schematics of the NACA 0012 airfoil model and MHFS arrays.

solid aluminum, with $C = 15$ cm and a span of 37.5 cm, was used in the investigation. A specially designed four-bar-linkage oscillation mechanism capable of oscillating the airfoil sinusoidally at large amplitude and frequency was used in the present experiment. The instantaneous angle of attack $\alpha(t)$ $(= \alpha_m + \Delta\alpha \sin \omega t$, where α_m is the mean angle of attack, $\Delta\alpha$ is the amplitude, $\omega = 2\pi f_0$ is the circular frequency, and t is the time) of the airfoil was recorded by using a potentiometer with an accuracy of ± 0.1 deg. Special emphases were placed on the oscillation conditions with oscillation amplitudes both within ($\alpha_m = 0$ deg and $\Delta\alpha = 5$ deg), through ($\alpha_m = 0$ deg and $\Delta\alpha = 11.5$ deg), and well beyond ($\alpha_m = 10$ deg and $\Delta\alpha = 15$ deg) α_{ss} (≈ 9 deg) for $Re_c (= U_\infty C/\nu$, where ν is the fluid kinematic viscosity) $= 1.95 \times 10^5$.

A total of 140 microthin (0.2 μm in thickness) multiple hot-film sensors (MHFS) with a sensor spacing S of 1.3 mm arranged in a straight-line array were used to identify the boundary-layer events. Each sensor consists of a nickel film 0.1 mm wide with 10-μm copper-coated nickel leads routed to provide wire attachment away from the measurement location (Fig. 1). Sensors S_1–S_{121} (S_{123}–S_{140}) were on the upper (lower) surface of the airfoil with sensor S_{122} located at the leading-edge stagnation point for $\alpha = 0$ deg. Groups of 16 of the 140 sensors were systematically connected to 16 AA Laboratory Model AN-1003 constant-temperature anemometers (CTAs) to obtain the time history of the heat transfer output at each sensor position. The overheat ratio and dc offset voltage for each hot-film sensor were carefully adjusted such that each sensor was at nearly the same operating conditions. The CTA output signals were sampled and digitized at 2 kHz on a 586 personal computer with a 12-bit A/D converter board. A four-channel spectral analyzer was also used to provide online time history traces and spectral contents of the operating groups. The output signals from the potentiometer were also sampled and served as reference signals between each set of CTA output signals. Details of the hot-film sensor arrays and their operation are given by Lee and Basu.[12]

Results and Discussion

Figure 2 shows the composite plot of selected simultaneously acquired multiple hot-film output signals (S_{124}–S_2) from the upper surface of the airfoil model oscillated with $\alpha_m = 0$ deg, $\Delta\alpha = 5$ deg, and $\kappa = 0.05$. The sensor numbers shown on the right-side ordinate axes in Fig. 2 indicate the distance, S/C, of the hot-film sensor from

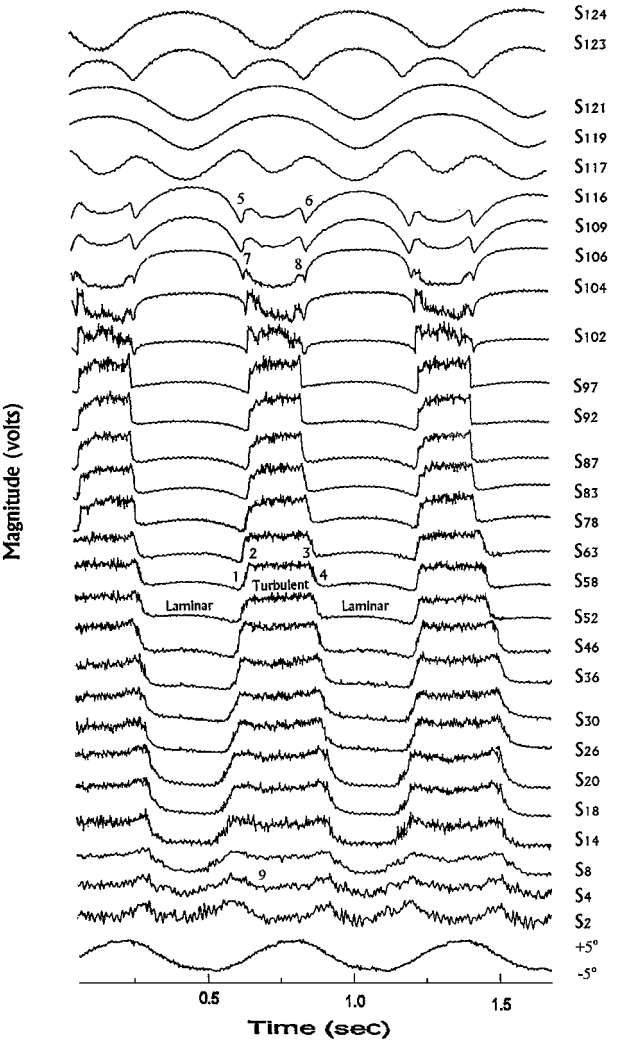

Fig. 2 Composite plots of selected simultaneously acquired hot-film outputs (S_{124}–S_2) for $\alpha(t) = 0 + 5 \sin \omega t$ deg and $\kappa = 0.05$; note that all of the sensor outputs are self-scaled instead of normalized by a common same voltage value.

the leading edge of the airfoil. The lowermost curve represents the variation in the potentiometer voltage. The y axes represent the self-scaled voltage output level of each sensor. Figure 2 reveals that, for an airfoil oscillated within α_{ss}, a portion of the boundary layer on the fully instrumented top surface (S_{104}–S_{14}) was initially laminar at the end of pitchdown ($\alpha_{min} = -5$ deg) and was always turbulent at the end of pitchup ($\alpha_{max} = +5$ deg) for each oscillation cycle and that the location of transition point (as indicated by a rapid increase in the sensor voltage level) moved forward along the airfoil during the pitchup. The subscript u indicates pitchup when α is increasing, and subscript d indicates pitchdown when α is decreasing. For clarity, the sensor output at S_{58} ($S/C = 0.554$) was selected to illustrate the state of the unsteady boundary layer. The onset of laminar-to-turbulent transition occurred at point 1 during pitchup. The turbulent boundary layer remained attached (between points 2 and 3) and relaminarized at point 4 during pitchdown. Figure 2 also shows that the turbulent boundary layer remains attached at least up to S_4 ($S/C = 1.023$), attributed to the favorable effects of unsteady motion, compared to $S/C = 0.953$ for a static airfoil[12] at $\alpha = 4.5$ deg. The self-scaled sensor outputs S_{116}–S_{106} (between points 5 and 6, which are associated with a rise and a drop in the heat transfer levels) and S_{104}–S_{102} (between points 7 and 8) suggest the existence of the laminar separation bubble and its bursting, respectively, during each oscillation cycle. The variations of the locations of the transition and relaminarization points with κ as a function of τ $(= \omega t)$ are summarized in Fig. 3.

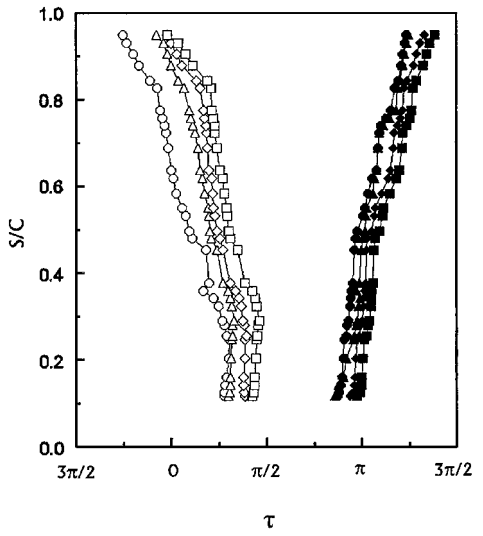

Fig. 3 Variation of the onset of boundary-layer transition and relaminarization with κ for $\alpha(t) = 0 + 5 \sin \omega t$ deg; transition: ○, $\kappa = 0.05$; △, $\kappa = 0.15$; ◇, $\kappa = 0.20$; □, $\kappa = 0.30$ and relaminarization: ●, $\kappa = 0.05$; ▲, $\kappa = 0.15$; ◆, $\kappa = 0.20$; ■, $\kappa = 0.30$.

Figure 3 reveals that the onset of transition (relaminarization) was delayed (promoted) with increasing (decreasing) κ during pitchup (pitchdown) motion, that is, the transition point moved toward the leading edge with increasing α_u and decreasing κ, and that the degree of asymmetry (or hysteresis) in the laminar–relaminarization cycle decreased slightly with increasing κ. The hysteresis is much stronger near the trailing edge (which could be attributed to the trailing-edge flow separation) than it is closer to the leading edge. Also, the variation in the length of the attached turbulent boundary layer is insensitive to κ. In summary, the primary influences of κ are to delay the forward motion of the transition point and to allow the turbulent boundary layer to withstand the imposed retardation, without suffering flow reversal, at substantially higher α than would be possible under static conditions. These stabilizing effects are attributed to the boundary-layer improvement effects (i.e., the accelerated-flow and moving-wall effects) in unsteady motions.[8,9]

Figure 4 shows the typical composite plot of the selected hot-film sensor (S_{123}–S_2) outputs for an airfoil model oscillated through α_{ss} with $\alpha_m = 0$ deg, $\Delta\alpha = 11.5$ deg, and $\kappa = 0.05$. By oscillating the airfoil through α_{ss} the surface flow conditions became more complicated compared to Fig. 2. Depending on the phase angle τ, the unsteady flow can be separating and reattaching over a small or large portion of the top surface of the airfoil. For example, the outputs of $S_{104}(S/C = 0.156)$ suggest that there is a separation or breakdown of the attached turbulent boundary layer (indicated by a drop in the sensor output voltage level) at point 1 ($\alpha_u \approx 10.5$ deg) during pitchup followed by a reattachment at 2 ($\alpha_d \approx 11.2$ deg) and the subsequent relaminarization at point 3 ($\alpha_d = 10.8$ deg) during pitchdown. Unlike the deep-stall case shown subsequently, the turbulent breakdown as indicated by points 4–12 in the outputs of S_{99}–S_8 ($S/C = 0.199$–0.988) indicates a trailing-edge flow separation. Similar to the steady trailing-edge stall, the reversed flow region expands upstream toward the leading edge. However, unlike for steady flow, for the unsteady case, flow reversal does not necessarily imply a significant departure of the boundary layer from the wall.[13] The effects of κ on the unsteady boundary-layer events for this light-stall oscillation case[11] are summarized in Fig. 5.

Figure 5 indicates that, for an airfoil oscillated through α_{ss} with $\kappa = 0.05$–0.30, 1) the trailing-edge turbulent separation is delayed to higher α_u with increasing κ, 2) an asymmetry (hysteresis) is also present for transition–relaminarization and separation–reattachment points, and 3) at a given chordwise position relaminarization generally occurred at a lower α than transition. In summary, also for relatively large-amplitude oscillation (i.e., light-stall case), the

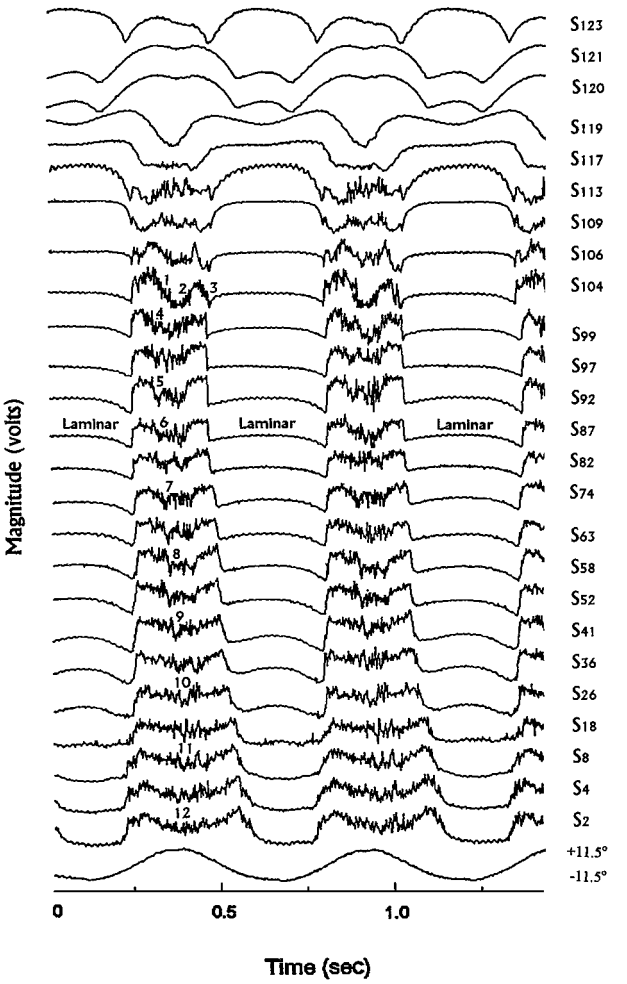

Fig. 4 Composite plot of selected simultaneously recorded hot-film signals (S_{124}–S_2) for $\alpha(t) = 0 + 11.5 \sin \omega t$ deg and $\kappa = 0.05$.

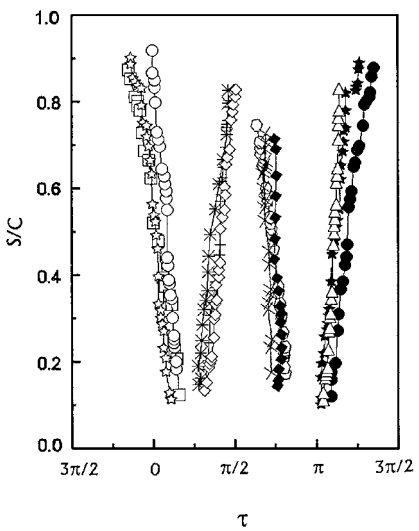

Fig. 5 Variation of the locations of transition and relaminarization, and separation and reattachment points with κ for $\alpha(t) = 0 + 11.5 \sin \omega t$ deg; transition: ☆, $\kappa = 0.05$; □, $\kappa = 0.15$; ○, $\kappa = 0.30$; relaminarization: ★, $\kappa = 0.05$; ◇, $\kappa = 0.15$; ●, $\kappa = 0.30$; separation: ∗, $\kappa = 0.05$; △, $\kappa = 0.15$; +, $\kappa = 0.30$; and reattachment: ×, $\kappa = 0.05$; ⬡, $\kappa = 0.15$; ◆, $\kappa = 0.30$ (note that only the clearly identifiable separation and reattachment points were plotted).

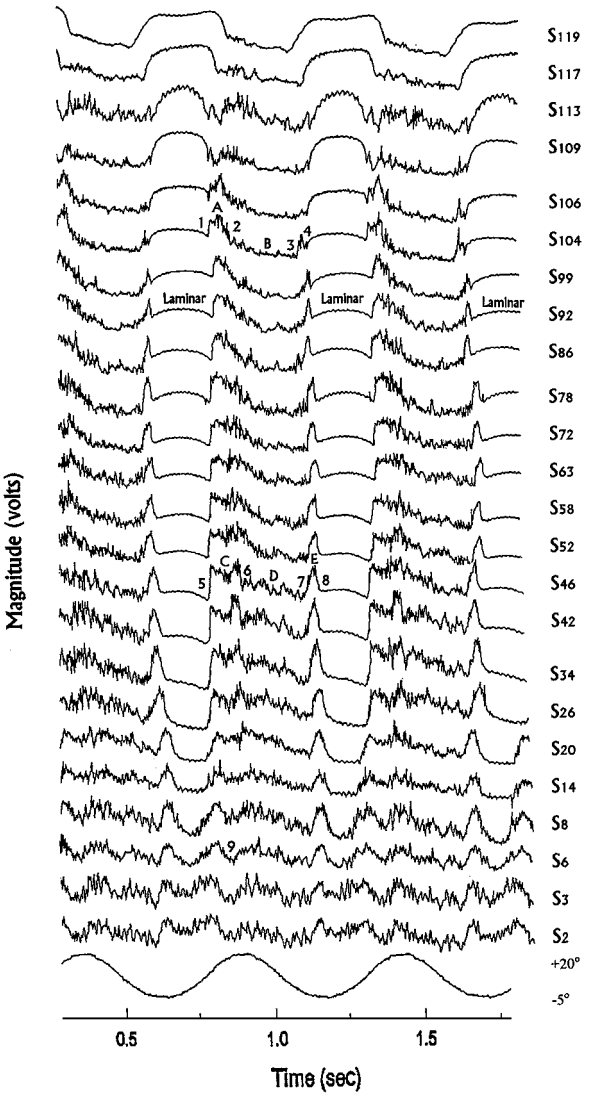

Fig. 6 Composite plot of selected hot-film signals (S_{119}–S_2) for $\alpha(t) = 10 + 15 \sin \omega t$ deg and $\kappa = 0.20$.

accelerated-flow and moving-wall effects delay the onset of trailing-edge separation and its rate of forward movement toward the leading edge.

Figure 6 shows the multiple hot-film sensor outputs for an airfoil oscillated well beyond α_{ss} with $\alpha_m = 10$ deg, $\Delta\alpha = 15$ deg, and $\kappa = 0.20$. The breakdown of the turbulent boundary layer in the leading-edge region, leading to the deep-stall phenomena as described by McCroskey[11] can be clearly identified. Starting at $S_{104}(S/C = 0.156)$, the boundary layer has undergone transition at point 1 ($\alpha_u = 10.5$ deg) and remained attached (region A). The turbulent boundary layer separated at point 2 or $\alpha_u \approx 21.2$ deg (indicated by a sudden breakdown or a drop in the heat transfer output level), which indicates the release of the leading-edge stall vortex (LEV). The detached boundary layer relaminarized at point 4 through a brief reattachment length (points 3 to 4) during pitchdown. The release and propagation of the LEV can be illustrated, for example, by the sensor outputs at $S_{46}(S/C = 0.506)$. The laminar boundary layer (up to point 5, $\alpha_u = 14.6$ deg) became turbulent (region C) and then broke down abruptly at point 6 ($\alpha_u \approx 20.2$ deg). The higher level of heat transfer of region D compared to that of region B indicates the high velocities induced by the LEV. The boundary layer became reattached (point 7, $\alpha_d \approx 6.9$ deg) and relaminarized (point 8, $\alpha_d \approx 2.5$ deg) at around the end of the pitchdown motion. Furthermore, near the trailing edge (S_{14}–S_1), the intermittent trailing-edge turbulent separation[10] (indicated by a minimum in the sensor output, for example, at point 9 or $\alpha_u \approx 20.8$ deg in the output of S_6) dominated.

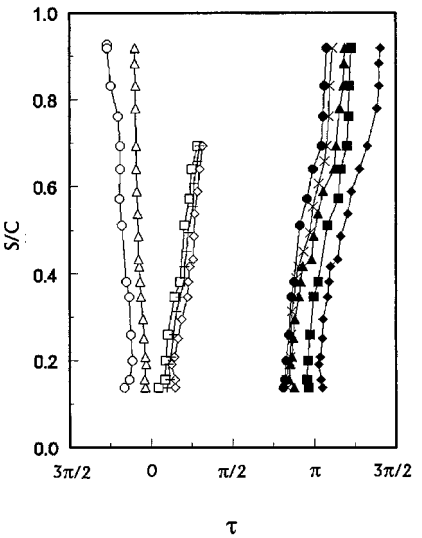

Fig. 7 Variation of boundary-layer events with κ for $\alpha(t) = 10 + 15 \sin \omega t$ deg; transition: ○, $\kappa = 0.10$; △, $\kappa = 0.30$; relaminarization: ■, $\kappa = 0.10$; ◆, $\kappa = 0.30$; separation: □, $\kappa = 0.10$; +, $\kappa = 0.20$; ◇, $\kappa = 0.30$; and reattachment: ●, $\kappa = 0.10$; ×, $\kappa = 0.20$; ▲, $\kappa = 0.30$ (note that only the clearly identifiable separation and reattachment points were plotted).

The increased heat transfer level suggests a lower trailing-edge-vortex convection speed compared to that of an LEV. The S_{119}–S_{109} outputs shows the existence of the laminar separation bubble and its bursting, which is consistent with the observations of Carr et al.[10] that the bubble bursting is the cause of the deep dynamic stall. The effects of κ on the spatial–temporal movement of the boundary-layer events for deep-stall oscillations are summarized in Fig. 7. Figure 7 shows that the rear-to-front progression and the delay (promotion) of the boundary-layer transition (relaminarization) with α are qualitatively similar to the results of Figs. 3 and 5 and that in the deep-stall region the vortex shedding from the airfoil is very similar, regardless of whether or not the flow separation at lower angles of attack was of the leading-edge or trailing-edge type.

Conclusions

The instantaneous locations of the unsteady boundary-layer transition, separation, and reattachment on an NACA 0012 airfoil oscillated sinusoidally at $Re_c = 1.95 \times 10^5$ were measured using MHFS. The boundary-layer transition and separation (relaminarization and reattachment) points were found to be delayed (promoted) with increasing (decreasing) reduced frequency during pitchup (pitchdown). Also, the deep dynamic stall process was originated with the turbulent leading-edge separation. These surface flow measurements contribute to the general understanding and control of unsteady flow separation over aerodynamic objects.

Acknowledgments

This work was supported by the National Sciences and Engineering Research Council of Canada. W. Zhou is thanked for his help on the design of the oscillation mechanism.

References

[1]McCroskey, W. J., Carr, L. W., and McAllister, K. W., "Dynamic Stall Experiments on Oscillating Airfoils," *AIAA Journal*, Vol. 14, No. 1, 1976, pp. 57–63.

[2]McAlister, K. W., and Carr, L. W., "Water Tunnel Visualizations of Dynamic Stall," *Journal of Fluids Engineering*, Vol. 101, 1979, pp. 376–380.

[3]Favier, D., Agnes, A., Barbi, C., and Maresca, C., "Combined Translational/Pitch Motion: A New Airfoil Dynamic Stall Simulation," *Journal of Aircraft*, Vol. 25, No. 9, 1988, pp. 805–814.

[4]Koochesfahani, M. M., "Vortical Patterns in the Wake of an Oscillating Airfoil," *AIAA Journal*, Vol. 27, No. 9, 1989, pp. 1200–1204.

[5]Lorber, P. F., Carta, F. O., and Covino, A. F., "Airfoil Dynamic Stall at Constant Pitch Rate and High Reynolds Number," *Journal of Aircraft*, Vol. 25, No. 3, 1988, pp. 548–556.

[6]Ohmi, K., Coutaneau, M., Daube, O., and Loc, T. P., "Further Experiments on Vortex Formation Around an Oscillating and Translating Airfoil at Large Incidences," *Journal of Fluid Mechanics*, Vol. 225, 1991, pp. 607–630.

[7]Fulgum, D. A., "Unmanned Strike Next for Military," *Aviation Week and Space Technology*, June 1997, pp. 49, 50.

[8]Ericsson, L. E., and Reding, J. P., "Fluid Mechanics of Dynamic Stall. Part I. Unsteady Flow Concept," *Journal of Fluids and Structure*, Vol. 2, No. 1, 1988, pp. 1–33.

[9]Ericsson, L. E., "Moving Wall Effect in Relation to Other Dynamic Flow Mechanics," *Journal of Aircraft*, Vol. 31, No. 6, 1994, pp. 1303–1309.

[10]Carr, L. W., McAlister, K. W., and McCroskey, W. J., "Analysis of the Development of Dynamic Stall Based on Oscillation Airfoil Experiments," NASA TN D-8382, Jan. 1977.

[11]McCroskey, W. J., "Unsteady Airfoils," *Annual Review of Fluid Mechanics*, Vol. 14, 1982, pp. 285–311.

[12]Lee, T., and Basu, S., "Measurement of Unsteady Boundary Layer Developed on an Oscillating Airfoil Using Multiple Hot-Film Sensors," *Experiments in Fluids*, Vol. 25, 1998, pp. 108–117.

[13]Sears, W. R., and Telionis, D. P., "Boundary Layer Separation in Unsteady Flow," *Journal of Applied Mathematics*, Vol. 23, No. 1, 1977, pp. 215–235.